Journal of Power Sources 195 (2010) 4206–4212

Contents lists available at ScienceDirect

Journal of Power Sources

journal homepage: www.elsevier.com/locate/jpowsour

A particle-layer model for solid-oxide-full-cell cathodes with different structures

Yanxiang Zhang, Changrong Xia*

Laboratory for Renewable Clean Energy, Department of Materials Science and Engineering, University of Science and Technology of China, 96 Jinzhai RD, Hefei, 230026 Anhui, China

ARTICLE INFO

Article history:
Received 15 December 2009
Received in revised form
19 December 2009
Accepted 22 December 2009
Available online 13 January 2010

Keywords:
Solid oxide full cells
Composite cathode
Polarization
Model

ABSTRACT

A particle-layer model is developed to quantitatively evaluate the electrochemical parameters of conventional composite cathodes (CCCs) and impregnated composite cathodes (ICCs) for solid oxide full cells (SOFCs). In this model, these cathodes are considered as a construction composed of particle layers. The parameters such as interfacial polarization resistance, three-phase boundary (TPB) length, and effective electrode thickness are formulated as a function of effective TPB resistivity, ionic resistivity, and cathode structure characteristics including electrode composition, porosity, particle size of electrocatalyst and electrolyte, and thickness. In addition, the model can be used as a convenient tool to estimate the effective TPB resistivity when the interfacial polarization resistance is available or experimentally determined. Furthermore, the ICC and CCC electrodes are theoretically compared. It is confirmed that the electrochemical performance can be significantly enhanced and small effective thickness can be reached by using ICC structure, compared with CCC, due to the remarkable enlargement of TPB length. The model also provides some strategies to design a high performance cathode.

1. Introduction

Cathodes in solid oxide fuel cells (SOFCs) are usually porous two-phase composites. By utilizing the composites as an alternative to porous single-phase cathodes, electrochemical reaction zones are extended from electrolyte/electrode interface to the bulk of the electrode [1] and the thermal expansion coefficient mismatch between the electrode and electrolyte layers is minimized [2]. These composite cathodes are often composed of an ionic conducting phase (the electrolyte), an electronic conducting phase (the electrocatalyst), and pores for gas transportation. They can be divided into two categories with different microstructures: (i) conventional composite cathodes (CCCs) and (ii) impregnated composite cathodes (ICCs). CCC is usually fabricated using a co-sintered process, starting with coating a mixture consisting of ionic and electronic particles onto a dense electrolyte layer using a slurry-based technique such as screen printing, followed by co-sintering the coated ionic and electronic particles at high temperatures. The resulted particle size of both phases is usually micrometer in scale due to the high-temperature sintering, which must be conducted to enhance the bonding strength between the cathode and electrolyte layers [3]. CCC structure is frequently considered as a random packing system consisting of spherical particles [4] as illustrated in Fig. 1a. Electrochemical reduction of oxygen molecule is usually believed to take place at so-called three-phase boundaries (TPBs), where percolated ionic particles, percolated electronic particles, and open pores contact with each other (Fig. 1c). A volume of experimental and simulation work suggests that large TPB length is necessary for high electrode performance and TPB is sensitive to the electrode geometric structure [3,5,6]. Unlike CCC, ICC is fabricated with separated sintered processes, where one-phase is screen-printed onto the electrolyte layer and sintered at high temperatures to achieve the strong bonding, while the other phase is deposited using an ion impregnation method and subsequently sintered at relatively low temperatures, resulting in much small particles, often nanometer in size [5]. Compared with CCC, TPB length of ICC is significantly enlarged due to the special geometric structure [3]. As shown in Fig. 1b, the ionic phase, which is prepared by high-temperature sintering, can be modeled as a random packing system of micron ionic particles, while the electronic phase, which is prepared by low-temperature sintering of ion-impregnates, can be regarded as a thin film composed of nanoscale electronic particles. Many experimental results indicate that significant performance enhancement can be obtained by utilizing the ICC structure [2,5,7,8]. For instance, Xu et al. [2] reported that, at 700 °C the interfacial polarization resistance decreases from 0.94 Ω cm^2 for a $(La_{0.85}Sr_{0.15})_{0.9}MnO_{3-\delta}$ (LSM)–$Ce_{0.8}Sm_{0.2}O_{1.9}$ (SDC) CCC to 0.35 Ω cm^2 for an ICC when the two electrodes have the same composition. It is believed that the coated nanoscale

* Corresponding author. Tel.: +86 5513607475; fax: +86 5513606689.
E-mail address: xiacr@ustc.edu.cn (C. Xia).

0378-7753/$ – see front matter © 2010 Elsevier B.V. All rights reserved.
doi:10.1016/j.jpowsour.2009.12.114

Nomenclature

A	geometric cross-sectional area of composite cathode, cm^2
A_{io-io}^{eff}	effective contact surface area between ionic particles per particle layer, μm^2
I_{io}	current through the cathode/electrolyte interface, A
L	cathode thickness, μm
L_{io-el}^{eff}	effective TPB length per particle layer, μm
P_{io}	percolation probabilities of ionic particles
P_{el}	percolation probabilities of electronic particles
P_{O_2}	oxygen partial pressure
R_{io}	ionic resistance per particle layer, Ω
R_{el}	electronic resistance per particle layer, Ω
R_{TPB}	resistance associated with oxygen reduction at TPBs per particle layer, Ω
R_p	interfacial polarization resistance, $\Omega\,cm^2$
r_{io}	radius of ionic particles, μm
r_{el}	radius of electronic particles, μm
r_{io-el}	smaller radius of ionic and electronic particles, μm
T	absolute temperature, K
v_{io}	number of ionic particles per unit volume, μm^{-3}
w	effective width of electrochemical active zone
x	coordinate along the cathode thickness, μm
Z_{io-io}	number of contacts between ionic particles
Z_{el-el}	number of contacts between electronic particles
Z_{io-el}	number of contacts between an ionic particle and electronic particles
$\overline{Z}$	average coordination number of all particles

Greek letters

Δ	radius ratio of electronic particles to ionic particles
δ_{io-io}	thickness of the ionic particle interface, nm
δ_{io-el}	effective thickness of electrochemical active zone
Φ_n^{io}	potentials of ionic conduction in the nth particle layer, V
Φ_n^{el}	potentials of electronic conduction in the nth particle layer, V
ϕ_{io}	volume fraction of ionic phase to the total solid materials
ϕ_{el}	volume fraction of electronic phase to the total solid materials
ϕ_g	porosity
ι	neck perimeter between an ionic particle and an electronic particle, μm
λ	effective cathode thickness, μm
μ	Bruggeman factor
θ	contact angle
ρ_{io}^{eff}	effective resistivity of ionic phase, $\Omega\,cm$
$\rho_{io,tra}^{eff}$	effective intra-particle resistivity of ionic phase, $\Omega\,cm$
$\rho_{io,ter}^{eff}$	effective inter-particle resistivity of ionic phase, $\Omega\,cm$
$\rho_{io,tra}^{o}$	intrinsic intra-particle resistivity of ionic phase, $\Omega\,cm$
$\rho_{io,ter}^{o}$	intrinsic inter-particle resistivity of ionic phase, $\Omega\,cm$
ρ_{TPB}^{eff}	effective resistivity at TPB, $\Omega\,cm$
ρ_{TPB}^{o}	intrinsic resistivity of electrochemical active zone, $\Omega\,cm$

particles enlarge the TPB length, leading to the decrease of polarization resistance. Zhu et al. [3] have indirectly confirmed this viewpoint theoretically by comparing the TPB length of the two type electrodes. However, due to the significant difference in the geometric structures of these cathodes, to the best of our knowledge, a theoretical model which is applicable to both CCC and ICC has not been proposed to estimate the cathode performance, yet. Most of the reported models focus on CCC [9,10], while a few of models are developed for ICC [11,12].

In this report, we try to develop a mathematical model to quantitatively assess the cathode performance in terms of interfacial polarization resistance for both ICC and CCC electrodes. In addition, the TPB length and effective thickness are calculated. Consequently, the performance enhancement mechanisms derived from the ion impregnation method are revealed. Some strategies are also outlined for fabricating high performance cathodes.

2. Model description

The composite electrodes, both ICC and CCC, are composed of spherical particles, which might have different sizes. It is therefore reasonable to consider that CCC and ICC are constructed by adding particles layer by layer onto the electrolytes. At each layer the resistance associated with the chemical/electrochemical reactions at TPB is the same. However, the resistance associated with concentration polarization and ionic–electronic conduction is different due to the different distance from the electrolyte to each layer. When the electrode porosity is high enough, usually ≥ 0.3, the concentration polarization resistance is negligible. So in one particle layer, the resistance for cathode reactions contains ionic resistance, R_{io}; electronic resistance, R_{el}; and resistance for reactions at TPBs, R_{TPB}, which is in series with R_{io} and R_{el}. Therefore, current transport through the ionic and electronic phases and reactions at TPBs can be modeled with the equivalent circuit as shown in Fig. 1d. In adjacent particle layers, the ionic conduction and electronic conduction connect, respectively. According to Kirchhoff's law of current, the governing equation for the conservation of ions and electrons in the nth particle layer is

$$\begin{cases} \dfrac{\Phi_n^{io}-\Phi_{n-1}^{io}}{R_{io}}+\dfrac{\Phi_n^{io}-\Phi_{n+1}^{io}}{R_{io}}+\dfrac{\Phi_n^{io}-\Phi_n^{el}}{R_{TPB}}=0 \\ \dfrac{\Phi_n^{el}-\Phi_{n-1}^{el}}{R_{el}}+\dfrac{\Phi_n^{el}-\Phi_{n+1}^{el}}{R_{el}}+\dfrac{\Phi_n^{el}-\Phi_n^{io}}{R_{TPB}}=0 \end{cases} \quad (1\text{-a})$$

where Φ_n^{io} and Φ_n^{el} denote the potentials for ionic and electronic conduction in the nth particle layer, respectively. However, due to the much low resistivity of the electronic phase (e.g., $7.8\times10^{-3}\,\Omega\,cm$ for LSM at 800 °C [1], and $5\times10^{-4}\,\Omega\,cm$ for $La_{0.6}Sr_{0.4}CoO_{3-\delta}$ (LSC) at 600 °C [13]) compared with that of ionic phase (e.g., $30\,\Omega\,cm$ for $Zr_{0.92}Y_{0.08}O_{1.96}$ (YSZ) at 800 °C [1], and $50\,\Omega\,cm$ for SDC at 600 °C [14]), the electronic resistance per particle layer is negligible. Consequently, the potential difference arising from the electronic phase is negligible. Thus Eq. (1-a) can be approximately degraded into

$$\frac{\Phi_n^{io}-\Phi_{n-1}^{io}}{R_{io}}+\frac{\Phi_n^{io}-\Phi_{n+1}^{io}}{R_{io}}+\frac{\Phi_n^{io}}{R_{TPB}}=0 \quad (1\text{-b})$$

The ionic resistance per particle layer can be estimated as

$$R_{io}=\rho_{io}^{eff}\frac{2r_{io}}{A} \quad (2)$$

where ρ_{io}^{eff}, $2r_{io}$, and A represent the effective resistivity of ionic phase, the thickness of one particle layer (the diameter of ionic particle), and the geometric cross-sectional area of composite cathode, respectively. Combining Eq. (1-b) with Eq. (2), the following

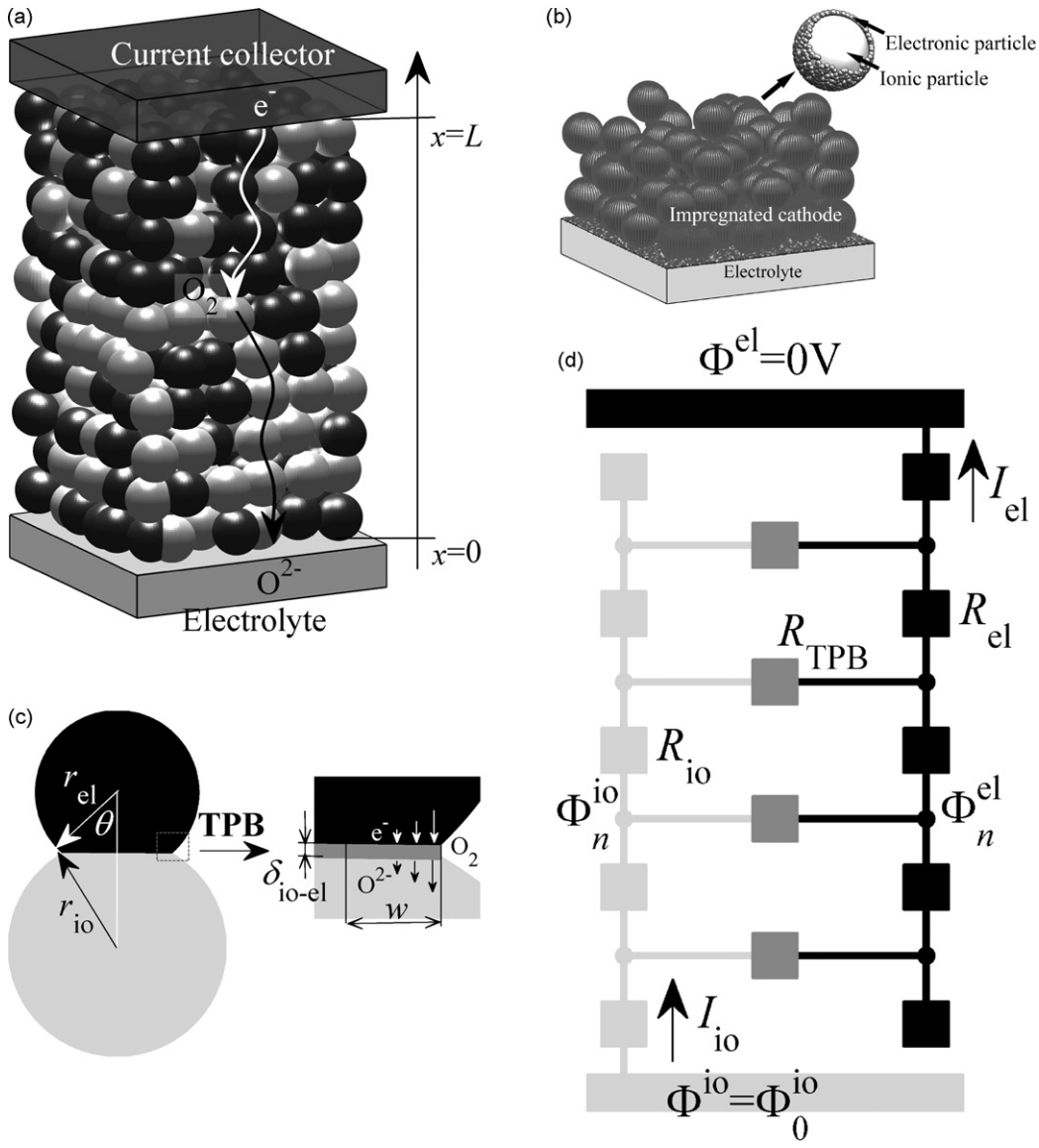

Fig. 1. Schematic geometric structure for the conventional composite cathode (CCC) (a), the impregnated composite cathode (ICC) (b), schematic illustrating the TPB (c), and the equivalent circuit of these composite cathodes composed of particle layers (d).

equation is obtained

$$\frac{A}{\rho_{\text{io}}^{\text{eff}} 2r_{\text{io}}}\left(\frac{\Phi_{n+1}^{\text{io}}-\Phi_{n}^{\text{io}}}{2r_{\text{io}}}-\frac{\Phi_{n}^{\text{io}}-\Phi_{n-1}^{\text{io}}}{2r_{\text{io}}}\right)=\frac{\Phi_{n}^{\text{io}}}{2r_{\text{io}}R_{\text{TPB}}} \tag{3}$$

Above equation can be mathematically re-written to

$$\frac{d^2}{dx^2}\Phi^{\text{io}}=\frac{\rho_{\text{io}}^{\text{eff}}}{2r_{\text{io}}AR_{\text{TPB}}}\Phi^{\text{io}} \tag{4}$$

where x is the coordinate along the cathode thickness (Fig. 1a). Assuming that the electrochemical reactions at cathode/electrolyte and current-collector/cathode interfaces are neglectable compared with those within the bulk of the composite electrode, the following boundary conditions are given

$$\Phi^{\text{io}}=\Phi_0^{\text{io}} \text{ for } x=0\,(n=0), \qquad \text{and} \qquad \frac{d\Phi^{\text{io}}}{dx}=0 \text{ for } x=L \tag{5}$$

where L is cathode thickness. Thus the potential in the ionic phase is presented as

$$\Phi^{\text{io}}=\frac{\Phi_0^{\text{io}}}{\exp(2L/\lambda)+1}\left[\exp\left(\frac{2L}{\lambda}-\frac{x}{\lambda}\right)+\exp\left(\frac{x}{\lambda}\right)\right] \tag{6}$$

where

$$\lambda=\sqrt{\frac{2r_{\text{io}}AR_{\text{TPB}}}{\rho_{\text{io}}^{\text{eff}}}} \tag{7}$$

The current through the cathode/electrolyte interface is

$$I_{\text{io}}=\frac{\Phi_0^{\text{io}}-\Phi_1^{\text{io}}}{R_{\text{io}}} \tag{8}$$

Combining Eqs. (6)–(8), the interfacial polarization resistance, R_{p}, is obtained

$$R_{\text{p}}=\rho_{\text{io}}^{\text{eff}}\lambda\coth\left(\frac{L}{\lambda}\right) \tag{9}$$

Above formulation is analogous to the thin film model developed by Kenjo et al. [15], which is an acursory quantitative analysis for the composite cathode since it neglects the electrode microstructure. In our model, the effect of cathode microstructure on the interfacial polarization can be discussed in detail and will be done in the following parts. When the cathode is very thick, Eq. (9)

may be approximated to

$$R_p = \rho_{io}^{eff}\lambda \tag{10}$$

The interfacial polarization resistance increases by 31.3% when the cathode thickness decreases from infinity to λ. Thus the parameter λ can be regarded as the effective thickness, which is a function of the effective resistivity of ionic phase and polarization resistance per particle layer as shown in Eq. (7). It should be noted this conclusion is made under the assumption that the electronic conduction resistance and concentration polarization resistance are negligible. However, it is of practical importance since λ is usually so small that the assumption is basically correct.

R_{TPB} is a function of geometric structures and oxygen reduction rate at TPBs as

$$R_{TPB} = \frac{\rho_{TPB}^{0}\delta_{io-el}}{wL_{io-el}^{eff}} \tag{11}$$

where ρ_{TPB}^{0} and L_{io-el}^{eff} represent the intrinsic resistivity for the oxygen reduction at the electrochemical active zone and the effective TPB length per particle layer, respectively. As shown in Fig. 1c, δ_{io-el} and w indicate the effective thickness and width of electrochemical active zone [16], respectively, which are usually not available. For simplification, an effective resistivity, ρ_{TPB}^{eff}, is practically defined for the reactions at TPB

$$\rho_{TPB}^{eff} \equiv \frac{\rho_{TPB}^{0}\delta_{io-el}}{w} \tag{12}$$

ρ_{TPB}^{eff} can be measured experimentally [9,17]. It is a constant if temperature and gas concentration are uniform throughout the cathode. Eq. (11) can be re-written as

$$R_{TPB} = \frac{\rho_{TPB}^{eff}}{L_{io-el}^{eff}} \tag{13}$$

L_{io-el}^{eff} is proportional to the neck perimeter per contact between an ionic particle and an electronic particle, ι; the volume of one particle layer, $2r_{io}A$; the number of ionic particles per unit volume, ν_{io}; the number of contacts between an ionic particle and electronic particles, Z_{io-el}; and the percolation probabilities of the ionic and electronic particles P_{io} and P_{el}. That is [4]:

$$L_{io-el}^{eff} = \iota\,(2r_{io}A)\,\nu_{io}Z_{io-el}P_{io}P_{el} \tag{14-a}$$

ι depends upon the smaller radius of ionic and electronic particles, r_{io-el}, and the contact angle, θ (Fig. 1c):

$$\iota = 2\pi r_{io-el}\sin\theta \tag{14-b}$$

It is widely assumed $\theta = \pi/12$ [3]. ν_{io} can be estimated as

$$\nu_{io} = \frac{(1-\phi_g)\phi_{io}}{4\pi r_{io}^3/3} \tag{14-c}$$

where ϕ_g represents the porosity and ϕ_{io} represents the volume fraction of ionic phase to the total solid materials.

For CCC, according to the percolation theory [4], Z_{io-el}, P_{io} and P_{el} can be estimated as

$$Z_{io-el} = \frac{\overline{Z}}{2}\left(1 + r_{io}^2/r_{el}^2\right)\frac{\phi_{el}/r_{el}}{\phi_{el}/r_{el} + \phi_{io}/r_{io}} \tag{14-d}$$

$$P_{io} = \left[1 - \left(\frac{4.236 - Z_{io-io}}{2.472}\right)^{2.5}\right]^{0.4} \tag{14-e}$$

$$P_{el} = \left[1 - \left(\frac{4.236 - Z_{el-el}}{2.472}\right)^{2.5}\right]^{0.4} \tag{14-f}$$

where $\overline{Z}$ is the average coordination number of all particles, which is widely assumed that $\overline{Z} = 6$. The coordination numbers among the same kind of particles are expressed as

$$Z_{io-io} = \overline{Z}\frac{\phi_{io}/r_{io}}{\phi_{el}/r_{el} + \phi_{io}/r_{io}} \tag{14-g}$$

$$Z_{el-el} = \overline{Z}\frac{\phi_{el}/r_{el}}{\phi_{el}/r_{el} + \phi_{io}/r_{io}} \tag{14-h}$$

For ICC, the ionic and electronic phases are continuous throughout the cathode, so P_{io} and P_{el} are both equal to 1. For the geometric structure illustrated in Fig. 1b, the ionic particles form a random packing system, thus Z_{io-io} equals to $\overline{Z}$. In case that the ionic particles are completely coated by the electronic particles, according to the model by Zhu et al. [3], the number of contacts between an ionic particle and electronic particles can be estimated as

$$Z_{io-el} = \frac{\left(6\cos\theta - 4\right)(1+\Delta)^3}{(1+\Delta)(1+2\Delta) - (1+2\Delta)^{1.5}} \tag{15}$$

where Δ is the radius ratio of electronic particles to ionic particles ($\Delta \equiv r_{el}/r_{io}$).

The effective resistivity of ionic phase is always expressed as the sum of intra-particle resistivity and inter-particle resistivity [4]:

$$\rho_{io}^{eff} = \rho_{io,tra}^{eff} + \rho_{io,ter}^{eff} \tag{16-a}$$

The intra-particle resistivity is estimated as

$$\rho_{io,tra}^{eff} = \frac{\rho_{io,tra}^{o}}{[(1-\phi_g)\phi_{io}P_{io}]^{\mu}} \tag{16-b}$$

where $\rho_{io,tra}^{o}$ is the intrinsic intra-particle resistivity. The Bruggeman factor μ is used to include the effects of tortuous conduction paths (μ is typically 1.5).

The inter-particle resistivity is evaluated as

$$\rho_{io,ter}^{eff} = \frac{\rho_{io,ter}^{o}\delta_{io-io}A}{2r_{io}A_{io-io}^{eff}} \tag{16-c}$$

where $\rho_{io,ter}^{o}$ is the intrinsic inter-particle resistivity, δ_{io-io} is the thickness of the ionic particle interface, about 5 nm [18]. A_{io-io}^{eff} is the effective contact surface area between ionic particles per particle layer:

$$A_{io-io}^{eff} = \pi(r_{io}\sin\theta)^2(2r_{io}A)\nu_{io}\frac{Z_{io-io}}{2}P_{io} \tag{16-d}$$

3. Results and discussion

3.1. Effective resistivities of TPB and ionic phase

To conduct the calculation, the effective resistivities of TPB and ionic phase should be available. This work takes the typical LSM–YSZ composite cathode as an example. With the reported data derived from the electrochemical measurements of LSM cathode on YSZ electrolyte [9], the effective resistivity of TPB can be obtained as the derivative of overpotential with respect to current per unit TPB length, given by

$$\rho_{TPB}^{eff} = 5.5\times10^{-7}{P_{O_2}}^{-1/4}T\,\exp\left(\frac{2.05\times10^4}{T}\right) + 6.0\times10^{-4}T\exp\left(\frac{1.24\times10^4}{T}\right) \tag{17}$$

The effective TPB resistivity is a function of oxygen partial pressure, P_{O_2}, and absolute temperature, T. In case $P_{O_2} = 0.21$, the effective TPB conductivity, $1/\rho_{TPB}^{eff}$, is $8.4\times10^{-8}\,S\,cm^{-1}$ at 600 °C and

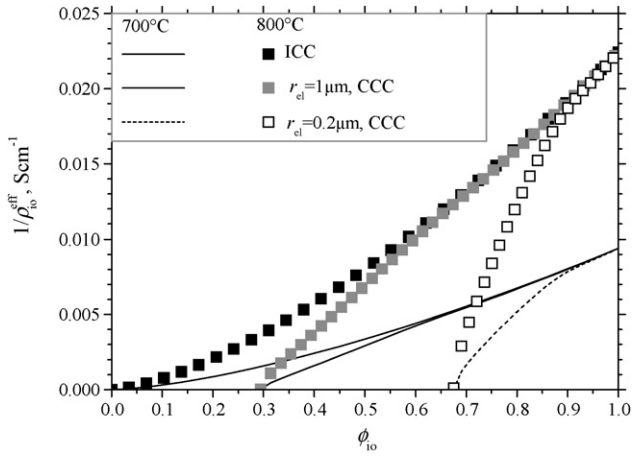

Fig. 2. The effective ionic conductivity, $1/\rho_{io}^{eff}$, as a function of YSZ volume fraction, ϕ_{io}, LSM particle size, r_{el}, and operating temperature, T (r_{io} = 1 μm, ϕ_g = 0.41).

4.2×10^{-6} S cm^{-1} at 800 °C. The results are consistent with the literature data of 4.0×10^{-6} S cm^{-1} at 800 °C, which is measured using electrochemical impedance spectroscopy and focused ion beam-scanning electron microscopy (FIB-SEM) [17].

While the effective TPB resistivity is the same for CCC and ICC, the effective ionic phase resistivities of CCC and ICC should be different due to their different microstructure. Arrhenius equation is applied to fit the experimental results of Ref. [19] to estimate the intrinsic intra-particle and inter-particle resistivity of YSZ as

$$\rho_{io,tra}^{o} = 1.5 \times 10^{-6} T \exp\left(\frac{1.0 \times 10^{4}}{T}\right) \quad (18\text{-a})$$

$$\rho_{io,ter}^{o} = 1.8 \times 10^{-5} T \exp\left(\frac{9.4 \times 10^{3}}{T}\right) \quad (18\text{-b})$$

Fig. 2 shows the effective YSZ conductivity, $1/\rho_{io}^{eff}$, as a function of YSZ volume fraction, ϕ_{io}, at different temperatures and particle sizes. For CCC, $1/\rho_{io}^{eff}$ is sensitive to LSM particle size. The smaller the LSM particle size, the larger the YSZ volume fraction should be utilized to achieve the same effective conductivity. Furthermore, there exists a volume fraction threshold for CCC. With the increase of YSZ volume fraction, $1/\rho_{io}^{eff}$ is zero below the threshold, increases sharply at the threshold, finally reaches the same value as that of ICC. On the contrary, ICC does not have the threshold. Its effective conductivity is independent of LSM particle size, much higher than that of CCC in low ϕ_{io} range, and is no less than that of CCC in the whole composition range when YSZ particles in CCC and ICC have the same size.

The practical composition of LSM–YSZ composite cathodes (CCC) is usually $\phi_{io} = \phi_{el}$. At this composition, according to the model calculation, the ionic conductivity for CCC is 7.0×10^{-3} S cm^{-1} at 800 °C, while it is 8.0×10^{-3} S cm^{-1} for ICC when $r_{io} = r_{el}$ = 1 μm and ϕ_g = 0.41. However, when r_{el} decreases to 0.2 μm, the conductivity for ICC is the same while it is neglectable for CCC since YSZ composition is below the percolation limit (Fig. 2). The difference in effective ionic conductivity between ICC and CCC is due to the percolation of YSZ particles. For ICC, the ionic particles are sintered with the electrolyte layers at high temperature to form YSZ backbones. Consequently, a continuous 3D network composed of YSZ particles is formed. While for CCC, the YSZ and LSM particles are mixed and co-sintered, resulting in a random packing system, so the continuity of YSZ particles is relative to the composition and the size of LSM particles.

The effective ionic conductivity is also strongly dependent on temperature. For instance, in case ϕ_{io} = 0.5, ϕ_g = 0.41 and r_{io} = 1 μm for ICC, $1/\rho_{io}^{eff}$ increases from 3.4×10^{-3} S cm^{-1} at 700 °C to 8.0×10^{-3} S cm^{-1} at 800 °C. The effective conductivity of ionic phase can be increased by using high operating temperature and/or ICC structure. But high operating temperature is not favorable to cost reduction.

3.2. TPB length of CCC and ICC

Fig. 3 shows the TPB length per unit volume, $L_{io-el}^{eff}/2r_{io}A$, as a function of YSZ volume fraction for different LSM particle sizes. For CCC, there exist lower and upper thresholds in terms of YSZ volume fractions, beyond which TPB length is negligible. The maximum TPB length per unit volume is reached at a certain YSZ volume fraction. For example, in case r_{io} = 1 μm, the maximum TPB length is obtained when YSZ volume fraction is 0.5 for r_{el} = 1 μm and 0.8 for r_{el} = 0.2 μm. This prediction is consistent with the literature data [6]. Fig. 3 also shows that remarkable TPB length enlargement can be obtained by utilizing ICC. The maximum TPB length for CCC with r_{el} = 0.2 μm is 1.3×10^{8} cm cm^{-3}. The TPB length increases to 8.0×10^{8} cm cm^{-3} for ICC when the coated LSM particle radius is 100 nm. It further increases to 34×10^{8} cm cm^{-3} when r_{el} decreases to 20 nm. The results imply that high cathode performance may be achieved with ICC even at relative low operating temperature due to their much high TPB length compared with that of CCC.

3.3. Interfacial polarization resistances of CCC and ICC

The validation of the particle-layer model is checked with literature data and the results are shown in Fig. 4. When CCC is operated at 950 °C, substituting the literature data [20] into our model, r_{io} = 0.25 μm, r_{el} = 0.5 μm, ϕ_g = 0.41 and L = 50 μm, the predicted interfacial polarization resistance is 0.16 Ω cm^2, compared with the literature data of 0.12 Ω cm^2 for the composition of 30 wt.% YSZ (ϕ_{io} = 0.31). When the operating temperature decreases from 950 °C to 700 °C, according to the model prediction, the polarization resistance increases from 0.12 Ω cm^2 to 2.12 Ω cm^2 when YSZ volume fraction is 0.42. For ICC with r_{io} = 1 μm, r_{el} = 75 nm, ϕ_g = 0.41, ϕ_{io} = 0.62 and L = 60 μm, the predicted polarization resistance is only 0.62 Ω cm^2 at 700 °C, close to the literature data of 0.48 Ω cm^2 [21], which is the only available data for ICC LSM–YSZ electrodes. It can be seen that the predicted resistance basically agrees with the experimental data for both CCC and ICC electrodes. The slight higher predicted resistances may be caused by neglecting

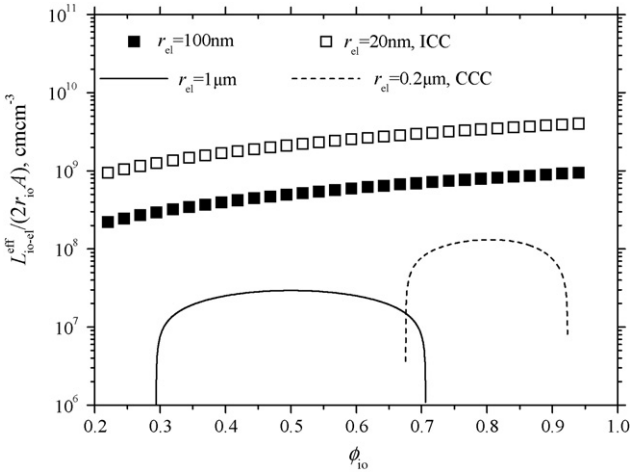

Fig. 3. TPB length per unit volume, $L_{io-el}^{eff}/2r_{io}A$, as a function of YSZ volume fraction, ϕ_{io}, and LSM particle size, r_{el} (r_{io} = 1 μm, ϕ_g = 0.41).

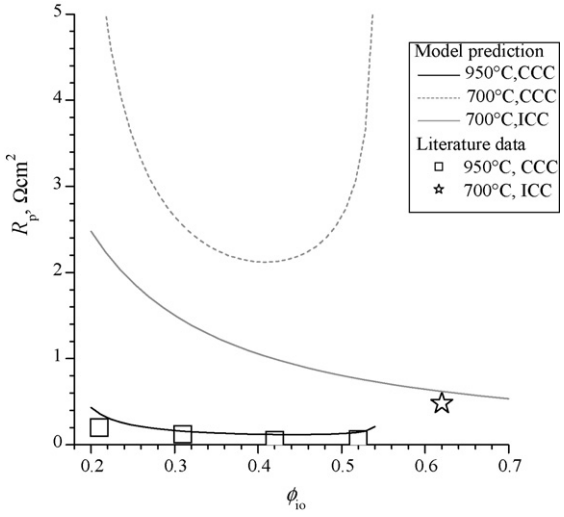

Fig. 4. Comparison between the model prediction and the literature data for CCC [20] and ICC [21].

the electrochemical reactions at cathode/electrolyte and current-collector/cathode interfaces.

As shown in Fig. 4, the predicted polarization resistance at the same temperature (700 °C) is much lower for ICC than that for CCC. The high electrochemical performance of ICC is due to the enlargement of TPB length (Fig. 3) as a result of the unique microstructures derived from the two-step sintering and ion-impregnation processes. Furthermore, for CCC, there exist lower and upper volume fraction threshold, at which the polarization resistance tends to be very large. This phenomenon is due to sharp decrease in TPB length at the thresholds. For ICC, the polarization resistance decreases with the increase of YSZ volume fraction when the porosity is fixed. It seems that the smaller the LSM volume fraction is, the lower the polarization resistance should be. However, the surface of YSZ particles might not be covered completely with the coated LSM particles when LSM volume fraction is low to a level where the electronic resistivity is not neglectable. In experiments, it is still a challenge to obtain continuous film-like structure by one-step impregnation. Contrarily, multi-step impregnation is necessary. It should be noted that excessive impregnation blocks gas diffusion, resulting in high concentration polarization resistance [22].

3.4. Effects of particle size

Normally, with the decrease of particle size, the performance can be improved due to the increase of TPB length, Fig. 5(a). The effective thickness is also relative to the TPB length per unit volume. Combining Eq. (7) with Eq. (13), the partial of λ with respect to $\ln\left(L^{\text{eff}}_{\text{io-el}}/2r_{\text{io}}A\right)$ is given by

$$\frac{\partial \ln(\lambda)}{\partial \ln\left(L^{\text{eff}}_{\text{io-el}}/2r_{\text{io}}A\right)} = -0.5 \tag{19}$$

Eq. (19) suggests that the thickness within which the electrochemical reaction takes place in ICC is smaller than that in CCC, Fig. 5(b). In addition, the effective thickness increases with the increase of particle size, which suggests that the larger the particle is used, the thicker the cathode should be fabricated. It should be noted that this suggestion is made under the assumption that the concentration polarization is negligible. Fig. 5(c) shows the polarization resistance as a function of the particle size. Decreasing particle size leads to significant increase in electrochemical performance. Unfortunately, for the-state-of-the-art CCC, the particles are usually micrometer in size due to the grain growth during the high-temperature sintering. But for ICC, the impregnated phase is usually introduced in the form of metal salts, so the sintering temperature is relative low, leading to a low level of grain growth. Thus, it is practical to achieve nano-sized particles by the impregnation technique, and substantially increase the performance.

3.5. Prediction of effective TPB resistivity

The particle-layer model can be used to calculate the effective TPB resistivity, $\rho^{\text{eff}}_{\text{TPB}}$, using the interfacial polarization resistances measured with either CCC or ICC. For example, according to the interfacial polarization resistances of LSM–YSZ CCCs with thicknesses of 5 μm and 11 μm [10], and the reported geometric parameters, such as $r_{\text{io}} = r_{\text{el}} = 0.15$ μm, $\phi_{\text{io}} = 0.5$ and $\phi_{\text{g}} = 0.4$, $\rho^{\text{eff}}_{\text{TPB}}$ is back-calculated as $(1.18 \pm 0.38) \times 10^7\ \Omega$ cm at 600 °C, $(1.79 \pm 0.61) \times 10^6\ \Omega$ cm at 700 °C, and $(3.45 \pm 1.18) \times 10^5\ \Omega$ cm at 800 °C, in accordance with that of $1.20 \times 10^7\ \Omega$ cm, $1.32 \times 10^6\ \Omega$ cm and $2.41 \times 10^5\ \Omega$ cm as obtained from Ref. [9] or Eq. (17), respectively. It implies that the effective TPB resistivity can be estimated by our model. Compared with the FIB-SEM reconstruction method [17], which is although the most accurate, this particle-layer model is much easier to conduct.

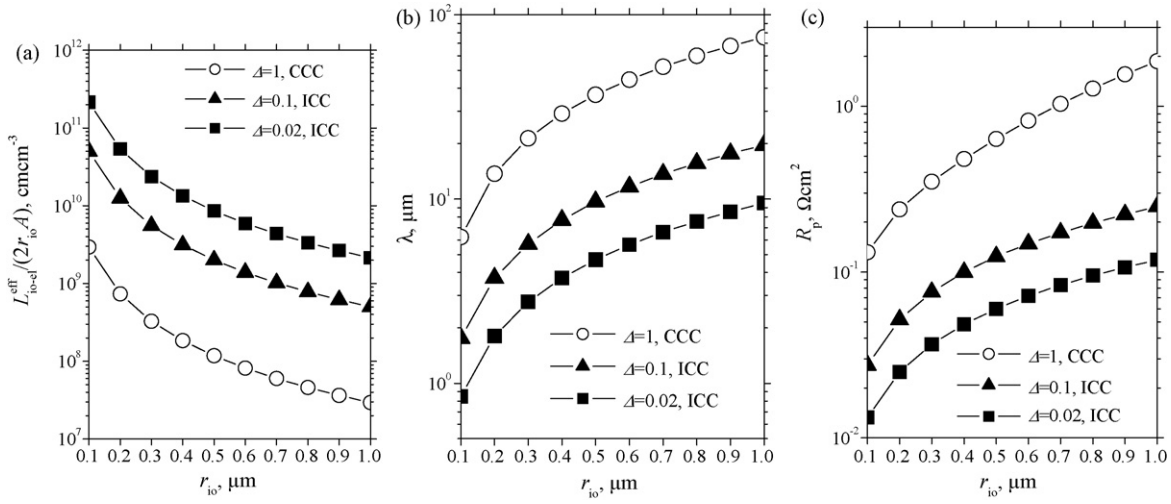

Fig. 5. TPB length per unit volume (a), $L^{\text{eff}}_{\text{io-el}}/2r_{\text{io}}A$, effective cathode thickness (b), λ, and polarization resistance (c), R_p, as a function of YSZ particle size, r_{io}, and particle size ratio, Δ, for CCC and ICC ($T = 800$ °C, $\phi_{\text{io}} = 0.5$, $\phi_{\text{g}} = 0.41$, $L = 50$ μm).

ρ_{TPB}^{eff} for LSC electrocatalyst on SDC electrolytes is not available in the literature. Based on the experimental data for the LSC–SDC cathodes [13], $\rho_{io,tra}^{o} = 50\,\Omega\,cm$ [14], $\rho_{io,ter}^{o} = 53\,\Omega\,cm$ [23] at 600 °C, using the reported geometric parameters, such as $r_{io} = 1\,\mu m$, $\phi_{io} = 0.5$ and $L = 50\,\mu m$, with $\phi_g = 0.41$ assumption, ρ_{TPB}^{eff} is estimated as $(4.2 \pm 0.34) \times 10^5\,\Omega\,cm$ according to the interfacial polarization resistances of $3.5\,\Omega\,cm^2$ and $0.31\,\Omega\,cm^2$ for the CCC with $r_{el} = 1\,\mu m$ and ICC with $r_{el} = 50\,nm$, respectively. The effective TPB resistivity is about two orders lower than that of the LSM–YSZ cathode on YSZ electrolyte. The difference in ρ_{TPB}^{eff} is possibly due to the difference catalytic activity with respect to surface oxygen exchange rates between LSM and LSC. For instance, the surface oxygen exchange coefficient at 800 °C is about $1.0 \times 10^{-8}\,cm\,s^{-1}$ for LSM [24], and $1.4–1.6 \times 10^{-5}\,cm\,s^{-1}$ for LSC [25]. In addition, due to the mixed oxygen-ionic and electronic conduction in LSC, the electrochemical active zone may be extended beyond TPB.

4. Conclusions

The TPB length, effective thickness, and interfacial polarization resistance for both CCC and ICC can be predicted using the particle-layer model developed in this work. Furthermore, the effective TPB resistivity can be estimated using the resistance data and geometric structure parameters of composite cathodes. According to the model calculation, compared with CCC, the sufficient decrease of the interfacial polarization resistance and the effective thickness of ICC are mainly due to the enlargement of the TPB length. The predicted results basically agree with the literature data. As a general trend, both for CCC and ICC, reasonably thicker cathode should be used to satisfy the demand of enough active sites for the electrochemical reaction when the particle size is bigger, which leads to the relative high effective thickness. Small connected-particle and low impregnation loading are critical to achieve a better performance using the ion impregnation method.

Acknowledgements

This work was supported by the Natural Science Foundation of China (10979046 and 50730002) and the Ministry of Science and Technology of China (2007AA05Z151).

References

[1] P. Costamagna, P. Costa, V. Antonucci, Electrochim. Acta 43 (1998) 375–394.
[2] X.Y. Xu, C.B. Cao, C.R. Ma, D.K. Peng, Ceram. Int. 35 (2009) 2213–2218.
[3] W. Zhu, D. Ding, C.R. Xia, Electrochem. Solid-State Lett. 11 (2008) B83–B86.
[4] D.F. Chen, Z.J. Lin, H.Y. Zhu, R.J. Kee, J. Power Sources 191 (2009) 240–252.
[5] S.P. Jiang, Mater. Sci. Eng. A 418 (2006) 199–210.
[6] S.H. Chan, X.J. Chen, K.A. Khor, J. Electrochem. Soc. 151 (2004) A164–A172.
[7] B. Wei, Z. Lü, X. Huang, M. Liu, K. Chen, W. Su, J. Power Sources 167 (2007) 58–63.
[8] S.P. Jiang, Y.J. Leng, S.H. Chan, K.A. Khor, Electrochem. Solid-State Lett. 6 (2003) A67–A70.
[9] X.J. Chen, S.H. Chan, K.A. Khor, Electrochim. Acta 49 (2004) 1851–1861.
[10] C. Nicolella, A. Bertei, M. Viviani, A. Barbucci, J. Appl. Electrochem. 39 (2009) 503–511.
[11] M. Shah, J.D. Nicholas, S.A. Barnett, Electrochem. Commun. 11 (2009) 2–5.
[12] J.D. Nicholas, S.A. Barnett, J. Electrochem. Soc. 156 (2009) B458–B464.
[13] F. Zhao, R.R. Peng, C.R. Xia, Mater. Res. Bull. 43 (2008) 370–376.
[14] D. Ding, B.B. Liu, Z. Zhu, S. Zhou, C.R. Xia, Solid State Ionics 179 (2008) 896–899.
[15] T. Kenjo, S. Osawa, K. Fujikawa, J. Electrochem. Soc. 138 (1991) 349–355.
[16] C.W. Tanner, K.Z. Fung, A.V. Virkar, J. Electrochem. Soc. 144 (1997) 21–30.
[17] J.R. Wilson, A.T. Duong, M. Gameiro, H.Y. Chen, K. Thornton, D.R. Mumm, S.A. Barnett, Electrochem. Commun. 11 (2009) 1052–1056.
[18] M.J. Verkerk, B.J. Middelhuis, A.J. Burggraaf, Solid State Ionics 6 (1982) 159–170.
[19] A.P. Santos, R.Z. Domingues, M. Kleitz, J. Eur. Ceram. Soc. 18 (1998) 1571–1578.
[20] J.D. Kim, G.D. Kim, J.W. Moon, Y.I. Park, W.H. Lee, K. Kobayashi, M. Nagai, C.E. Kim, Solid State Ionics 143 (2001) 379–389.
[21] Y.Y. Huang, J.M. Vohs, R.J. Gorte, J. Electrochem. Soc. 152 (2005) A1347–A1353.
[22] D. Ding, W. Zhu, J.F. Gao, C.R. Xia, J. Power Sources 179 (2008) 177–185.
[23] Z. Zhan, T.L. Wen, H. Tu, Z.Y. Lu, J. Electrochem. Soc. 148 (2001) A427–A432.
[24] Y. Ji, J.A. Kilner, M.F. Carolan, Solid State Ionics 176 (2005) 937–943.
[25] W. Preis, E. Bucher, W. Sitte, J. Power Sources 106 (2002) 116–121.